Available online at www.sciencedirect.com
SCIENCE DIRECT®
Journal of Sound and Vibration 276 (2004) 957–979
JOURNAL OF SOUND AND VIBRATION
www.elsevier.com/locate/jsvi

Modal parameter estimation from input–output Fourier data using frequency-domain maximum likelihood identification

P. Verboven*, P. Guillaume, B. Cauberghe, S. Vanlanduit, E. Parloo

Department of Mechanical Engineering (TW-WERK), Acoustics and Vibration Research Group, Vrije Universiteit Brussel, Pleinlaan 2, B-1050 Brussels, Belgium

Received 1 April 2003; accepted 7 August 2003

Abstract

A multi-variable frequency-domain maximum likelihood estimator is proposed to identify the modal parameters together with confidence intervals directly from the input–output Fourier data. The use of periodic excitation signals enables the use of a so-called non-parametric errors-in-variables noise model for an accurate description of the measurement set-up. The combination with a maximum likelihood identification approach yields a solver that is extremely robust to errors in the data, such as noise and leakage and hence results in accurate models. Since the maximum likelihood approach involves an optimization problem, a least-squares estimator is proposed as well, with the availability of a stabilization diagram. Both algorithms have been optimized for modal analysis applications by a significant reduction of the computation time and memory requirements. In the case when random noise excitation is required, the proposed method allows a parametric compensation for effects of leakage.

1. Introduction

The common approach for experimental modal identification starts from frequency response functions (FRF), which are derived using a non-parametric FRF estimator such as H_1 or H_v [1] (see Appendix A for list of abbreviations). Next, the modal parameters are estimated using curve fitting schemes, such as the Prony scheme [1,2], eigensystem realization (ERA) [3] or rational fractional polynomial (RFP) algorithms [4,5]. One of the most popular identification schemes used in the industry consists of a two-step approach [6]. First the poles and modal participation

*Corresponding author. Tel.: +32-2-629-28-07; fax: +32-2-629-28-65.
E-mail address: peter.verboven@vub.ac.be (P. Verboven).

0022-460X/$ - see front matter
doi:10.1016/j.jsv.2003.08.044

factors are estimated with the polyreference LSCE estimator (based on the Prony scheme) for different model orders and poles are selected from a stabilization chart. In the second step, the poles are fixed in the modal model and the mode shapes are estimated by means of a least-squares frequency-domain (LSFD) solver [2].

However, traditional modal analysis can be hampered by one or more of the following problems:

- As a first step, FRF estimation is most often performed using the H_1 FRF estimator. However, over-restrictive assumptions about the noise model, i.e., only noise present on the responses, results in inconsistent FRF estimation, which implies a bias error on the FRF estimates. Introducing a non-parametric errors-in-variables (EV) noise model [7,8] yields an improved representation of the measured data by considering errors both on the force and response observations. The proposed ML estimator is based on the errors-in-variables formulation starting from the Fourier series of the measured force and response signals (i.e., the input–output data). Accurate FRF estimation is also possible based on EV non-parametric estimators, such as the H_{iv} (arbitrary excitation [9,10]) or H_{ev} (periodic excitation [8]).
- Another problem relates to the use of arbitrary excitation signals (e.g., random noise) which introduces effects of leakage, especially when only short time sequences can be obtained from lightly damped structures. Even when time windowing (e.g., Hanning) is applied, both the effects of leakage and the window itself can result in significant errors on the modal parameters (especially the modal damping). Random noise excitation is often still used in modal testing since possible non-linear distortions are reduced by averaging. However, periodic signals, such as multisine or periodic chirp signals, avoid effects of leakage and generally result in signals of better quality. The proposed ML estimator will be evaluated using both random and periodic excitation signals.
- FRF data is commonly accepted as the starting point for modal analysis and the main reasons are the use of averaging to reduce noise on the data as well as to retain a more compact data set. Nevertheless, in the case when periodic excitation is applied, the same benefits are retained by averaging the Fourier spectra of the measured force and response signals (denoted as IO data). In addition, starting directly from the force and response Fourier data avoids FRF computation, which can be hampered by the effect of drops in the force signal, due to for example, an interaction between the structure and the excitation devices. This can result in important errors especially in the case of mechanical structures with a high dynamical range. The proposed ML estimator starts from the IO data and will be compared to its FRF-based equivalent discussed in Ref. [11].
- Generally, the commonly used curve fitting schemes are not able to handle noisy measurements and often result in unclear stabilization plots, which hampers the mode selection process. However, by a better exploitation of the information in the data, more information can be extracted in terms of the uncertainty on the data. In practice, the coherence function is well known as a measure for the quality of an FRF. Nevertheless, traditional curve fitting schemes never take this information into account during the parametric identification. On the other hand, the proposed ML estimator is specifically developed to improve parameter estimation by taking the uncertainty on the measured data into account.

In Refs. [8,12] a frequency-domain maximum likelihood (ML) algorithm is presented for parametric identification of both single input single output (SISO) and multiple input multiple output (MIMO) models from IO data. The formulation of the IO estimators is based on an errors-in-variables noise model, where both the errors on the input and output signals are considered. One of the drawbacks of maximum likelihood solvers which are often referred to is their computational load for large amounts of data. In the present contribution, the numerical performance (computation time, memory usage and numerical conditioning) of frequency-domain ML techniques is optimized to handle extensive modal data sets characterized by a high modal density. Furthermore, the proposed IO ML estimator is made robust for effects of leakage, when applying arbitrary excitation, by estimating simultaneously the initial conditions and the system model parameters.

2. Parametric frequency-domain identification

2.1. Parametric model

In this paper, a common denominator model is used to model the frequency response function between output o and input i (for $o = 1, 2, \ldots, N_o$ and $i = 1, 2, \ldots, N_i$) at angular frequency ω_f with $f = 1, \ldots, N_f$ (N_f the number of spectral lines)

$$\hat{H}_{oi}(\omega_f) = \frac{B_{oi}(\Omega_f, \theta)}{A(\Omega_f, \theta)}, \tag{1}$$

with $B_{oi}(\Omega_f, \theta) = \sum_{j=0}^{n} b_{oij}\Omega_f^j$ the numerator polynomial and $A(\Omega_f, \theta) = \sum_{j=0}^{n} a_j\Omega_f^j$ the common-denominator polynomial, where n is the order of the polynomials (which can differ for both polynomials) and Ω_f the generalized transform variable. In this case, a discrete-time domain model is used, where the generalized transform variable Ω_f, evaluated at the discrete Fourier transform frequency f, is then given by $\Omega_f = e^{(-i\omega_f T_s)}$ (Z-domain) with T_s the sampling period. The polynomial coefficients a_j and b_{oij} are the parameters θ to be estimated. Other choices are possible such as for example $\Omega_f = (-i\omega_f/\omega_S)$ for a continuous-time domain model (with $\omega_S = (\omega_1 + \omega_{N_f})/2$ a scaling factor used to improve numerical conditioning) or orthogonal Forsythe polynomials.

2.2. Errors-in-variables noise model

In practice, the measured responses (velocities and/or accelerations) as well as forces are affected by errors, i.e., measurement noise and process noise (due to environmental influences which act as non-measured forces on the structure). Hence, as shown in Fig. 1, the measured IO Fourier data $\mathbf{Z} = [\mathbf{F}^H, \mathbf{X}^H]^H$ can be represented using an *errors-in-variables* stochastic noise model

$$\begin{aligned} &\mathbf{Z}(\omega_f) = \mathbf{Z}_0(\omega_f) + \mathbf{E}_Z(\omega_f), \\ &[\mathbf{H}_0(\omega_f), -\mathbf{I}_{N_o}]\mathbf{Z}_0(\omega_f) = 0, \end{aligned} \quad f = 1, \ldots, N_f, \tag{2}$$

with $\mathbf{Z}_0 = [\mathbf{F}_0^H, \mathbf{X}_0^H]^H$ the "*true*" input–output (IO) Fourier data and $\mathbf{E}_Z = [\mathbf{E}_F^H, \mathbf{E}_X^H]^H$ some random perturbations, where $\mathbf{Z}(\omega_f)$, $\mathbf{Z}_0(\omega_f)$, $\mathbf{E}_Z(\omega_f) \in \mathbb{C}^{(N_i+N_o\times 1)}$.

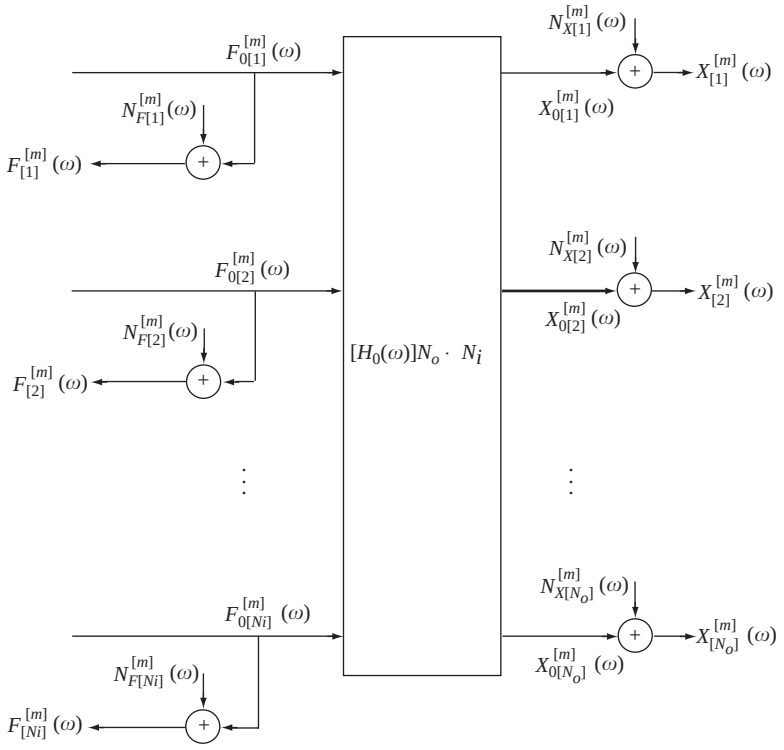

Fig. 1. Frequency-domain errors-in-variables noise model.

The errors $\mathbf{E}_Z(\omega_f)$ are assumed to be complex normally distributed with the following a priori known covariance matrix

$$\mathbf{C}_{E_Z}(\omega_f) = \mathscr{E}\{\mathbf{E}_Z(\omega_f)\mathbf{E}_Z(\omega_f)^{\mathrm{H}}\} = \begin{pmatrix} \mathbf{C}_{E_F}(\omega_f) & \mathbf{C}_{E_F E_X}(\omega_f) \\ \mathbf{C}_{E_X E_F}(\omega_f) & \mathbf{C}_{E_X}(\omega_f) \end{pmatrix}, \tag{3}$$

where the non-diagonal elements of the output noise covariance matrix $\mathbf{C}_{E_X}$ are not considered throughout this work. This follows from the practical issues related to the derivation of a full rank covariance matrix $\mathbf{C}_{E_Z}(\omega_f)$ for a large number of responses (N_o), which requires that the number of measurements is minimally equal to the number of responses. Furthermore, a time-efficient implementation of the IO estimators requires that $\mathbf{C}_{E_X}$ is diagonal as will be shown.

On the other hand, since the number of inputs is typically small ($N_i \leqslant 5$), input correlations as well as input–output correlations can be determined, resulting in $\mathbf{C}_{E_F}(\omega_f)$ and $\mathbf{C}_{E_X E_F}(\omega_f)$ being full matrices for each measured output. Taking into account, besides the noise variances, the cross-correlations of the errors on the IO data as well, can further decrease the uncertainty of the estimates.

For the particular case of scanning laser Doppler vibrometer (SLDV) measurements, the errors on the (subsequent) output measurements are uncorrelated since each response location is measured separately resulting in zero non-diagonal elements of $\mathbf{C}_{E_X}(\omega_f)$, and hence an exact noise model will be used for an SLDV setup.

2.3. Maximum likelihood identification from input–output data

Using the common denominator model (1) and given the IO data as defined in Eq. (2), the linearized equation error for output o and spectral line f is then written as the following scalar expression:

$$\varepsilon_o(\Omega_f,\theta) = \lfloor \mathbf{B}_o(\Omega_f,\theta) \rfloor \{\mathbf{F}(\omega_f)\} - A(\Omega_f,\theta)X_o(\omega_f), \tag{4}$$

where $\{\mathbf{F}(\omega_f)\}$ represents the input $(N_i \times 1)$ Fourier vector and X_o the output Fourier coefficient measured at degree of freedom (d.o.f.) o for spectral line f as a result of the N_i inputs. The $(1 \times N_i)$ row vector $\lfloor \mathbf{B}_o(\Omega_f,\theta) \rfloor$ is the oth row of the $(N_o \times N_i)$ numerator polynomial matrix $\mathbf{B}(\Omega_f,\theta)$. Notice that in the specific case of SLDV measurements, a different input Fourier vector $\{\mathbf{F}_o(\omega_f)\}$ is measured for each output d.o.f.

Based on the *weighted* equation error $\varepsilon_o^s(\Omega_f,\theta) = \varepsilon_o(\Omega_f,\theta)\,\mathrm{var}(\varepsilon_o(\Omega_f,\theta))^{-1/2}$ the ML cost function is given by

$$\begin{aligned}\ell_{ML}(\theta) &= \sum_{o=1}^{N_o}\sum_{f=1}^{N_f} \varepsilon_o^s(\Omega_f,\theta)\varepsilon_o^{s*}(\Omega_f,\theta) \\ &= \sum_{o=1}^{N_o}\sum_{f=1}^{N_f} \frac{|\lfloor \mathbf{B}_o(\Omega_f,\theta) \rfloor \{\mathbf{F}_o(\omega_f)\} - A(\Omega_f,\theta)X_o(\omega_f)|^2}{\mathrm{var}(\varepsilon_o(\Omega_f,\theta))},\end{aligned} \tag{5}$$

where the variance of the equation error (4) is given as

$$\begin{aligned}\mathrm{var}(\varepsilon_o(\Omega_f,\theta)) = {} & \lfloor \mathbf{B}_o(\Omega_f,\theta) \rfloor \mathbf{C}_{E_F}(\omega_f) \lfloor \mathbf{B}_o(\Omega_f,\theta) \rfloor^{\mathrm{H}} + |A(\Omega_f,\theta)|^2\,\mathrm{var}(X_o(\omega_f)) \\ & - 2herm(\lfloor \mathbf{B}_o(\Omega_f,\theta) \rfloor \mathbf{C}_{E_F E_X[:,o]}(\omega_f) A(\Omega_f,\theta)^*),\end{aligned} \tag{6}$$

with $\mathbf{C}_{E_F E_X[:,o]}(\omega_f)$ the oth column of the matrix $\mathbf{C}_{E_F E_X}(\omega_f)$ in Eq. (3).

2.4. Frequency-domain identification in the presence of transient phenomena

A typical problem for frequency-domain estimators in general arises from the presence of *transient phenomena* in the data, of which spectral *leakage* is an important example. Problems of leakage are avoided when the signals are acquired using an excitation signal that is periodic or time limited within the observation window as in the case of e.g., an impulse or burst random excitation. However, when random noise excitation is required, the applicability of frequency-domain modal parameter estimation from IO data can be generalized to arbitrary signals based on [13].

When the modal parameters are derived directly from the IO data there is in general a difference between time- and frequency-domain methods. This difference is mainly due to the manner in which the initial conditions of the system are taken into account. This can be understood by considering the Laplace transform of the jth derivative of the force time signal $f(t)$ of a SISO system

$$L\left\{\frac{\mathrm{d}^j f(t)}{\mathrm{d}t^j}\right\} = s^j F(s) - \sum_{r=0}^{j-1} s^{j-1-r} \left.\frac{\mathrm{d}^r f(t)}{\mathrm{d}t^r}\right|_{t=0}, \tag{7}$$

where the sum is a polynomial in the Laplace variable of order $(j-1)$ which only exists if the initial conditions differ from zero. Hence, when taking the initial conditions into account, the Laplace transformed SISO input–output differential equation is given as

$$A(s)X(s) = B(s)F(s) + T(s), \tag{8}$$

where the order of $T(s)$ equals the maximum order of $B(s)$ and $A(s)$ minus 1 with unknown coefficients $\theta_T = [c_0, c_1, \ldots, c_{n-1}]^{\mathrm{T}}$.

From this it follows that a *transient polynomial* $T(\Omega_f, \theta)$ can be used to model the initial conditions (e.g., the effects of leakage) present in the IO data. For example in the case of the ML estimator, adding the polynomial $T(\Omega_f, \theta)$ to the equation error ε_o results in the following generalized cost function:

$$\ell_{ML}(\theta) = \sum_{o=1}^{N_o} \sum_{f=1}^{N_f} \frac{\left| \lfloor \mathbf{B}_o(\Omega_f, \theta), T(\Omega_f, \theta) \rfloor \begin{Bmatrix} \{\mathbf{F}(\omega_f)\} \\ 1 \end{Bmatrix} - A(\Omega_f, \theta) X_o(\omega_f) \right|^2}{\mathrm{var}(\varepsilon_o(\Omega_f, \theta))}. \tag{9}$$

The (unknown) coefficients of $T(\Omega_f, \theta)$ are included in θ and are estimated simultaneously with the coefficients of $\mathbf{B}(\Omega_f, \theta)$ and $A(\Omega_f, \theta)$. This result indicates that taking a '*transient*' polynomial into account is equivalent with having one additional input with a constant Fourier spectrum equal to 1, and as a result, the same IO algorithms can still be applied. Hence, parametric frequency-domain estimators can be made robust for leakage by estimating the initial (and final) conditions together with the system parameters.

3. Fast implementation of ML algorithm

Before presenting the frequency-domain ML algorithm, first the least-squares (LS) solver for modal parameter estimation from IO data will be explained. This LS estimator will serve as a starting value generator or as stand-alone method with a stabilization diagram. The techniques used to optimize the computational efficiency will be explained for the LS and can be easily generalized for the ML estimator.

3.1. (Weighted) linear least-squares solver

Since Eq. (4) is linear in the parameters and in the Fourier data, it can be formulated as $\mathbf{J}\theta \approx 0$

$$\begin{bmatrix} \mathbf{\Gamma}_1 & 0 & 0 & \cdots & \mathbf{\Phi}_1 \\ 0 & \mathbf{\Gamma}_2 & 0 & \cdots & \mathbf{\Phi}_2 \\ \vdots & \vdots & \ddots & \vdots & \vdots \\ 0 & 0 & \cdots & \mathbf{\Gamma}_{N_o} & \mathbf{\Phi}_{N_o} \end{bmatrix} \begin{Bmatrix} \theta_{B_1} \\ \theta_{B_2} \\ \vdots \\ \theta_{B_{N_o}} \\ \theta_A \end{Bmatrix} \approx 0, \tag{10}$$

with $\mathbf{J}$ the Jacobian matrix now having $N_f N_o$ rows and $(n+1)(N_o N_i + 1)$ columns. A similar formulation can be obtained for real coefficients for which the number of equations and coefficients is then doubled. The entries of the submatrices $\mathbf{\Gamma}_o = [\mathbf{\Gamma}_{o1}, \ldots, \mathbf{\Gamma}_{oN_i}]$ $(N_f \times N_i.(n+1))$

and $\mathbf{\Phi}_o$ ($N_f \times (n+1)$) are given by

$$\begin{aligned}\mathbf{\Gamma}_{oi}(\omega_f) &= \mathrm{W}_o(\omega_f)[\Omega_f^0, \Omega_f^1, \ldots, \Omega_f^n]F_i(\omega_f),\\ \mathbf{\Phi}_o(\omega_f) &= -\mathrm{W}_o(\omega_f)[\Omega_f^0, \Omega_f^1, \ldots, \Omega_f^n]X_o(\omega_f),\end{aligned} \tag{11}$$

while the parameter vector entries contain the (unknown) coefficients

$$\begin{aligned}\theta_{B_o} &= [b_{o10}, b_{o11}, \ldots, b_{oN_in}]^{\mathrm{T}}, \quad o = 1, \ldots, N_o,\\ \theta_A &= [a_0, a_1, \ldots, a_n]^{\mathrm{T}}.\end{aligned} \tag{12}$$

An adequate (frequency-dependent) weighting function $\mathrm{W}_o(\omega_f)$ in Eq. (4), generally improves the quality of the parameter estimates (see Section 4).

However, since the number of measured frequencies N_f is typically large for modal testing (i.e., $N_f \gg n$), the LS formulation based on the so-called *normal equations* $\mathbf{J}^{\mathrm{H}}\mathbf{J}\theta \approx 0$ results in a more compact formulation of the identification problem ($\mathbf{J}^{\mathrm{H}}\mathbf{J}$ having $(n+1)(N_o.N_i+1)$ rows and columns)

$$\begin{bmatrix} \mathbf{R}_1 & 0 & \cdots & \mathbf{S}_1 \\ 0 & \mathbf{R}_2 & 0 & \mathbf{S}_2 \\ \vdots & 0 & \ddots & \vdots \\ \mathbf{S}_1^{\mathrm{H}} & \mathbf{S}_2^{\mathrm{H}} & \cdots & \sum_{o=1}^{N_o} \mathbf{T}_o \end{bmatrix} \begin{Bmatrix} \theta_{B_1} \\ \theta_{B_2} \\ \vdots \\ \theta_{B_{N_o}} \\ \theta_A \end{Bmatrix} \approx 0, \tag{13}$$

with $\mathbf{R}_o$ having $(n+1)N_i$ rows and columns, $\mathbf{S}_o$ having $(n+1)N_i$ rows and $(n+1)$ columns, and $\mathbf{T}_o$ having $(n+1)$ rows and columns, where

$$\mathbf{R}_o = \begin{bmatrix} \mathbf{R}_o^{11} & \cdots & \mathbf{R}_o^{1N_i} \\ \mathbf{R}_o^{21} & \cdots & \mathbf{R}_o^{2N_i} \\ \vdots & \ddots & \vdots \\ \mathbf{R}_o^{N_i1} & \cdots & \mathbf{R}_o^{N_iN_i} \end{bmatrix} \quad \text{and} \quad \mathbf{S}_o = [\mathbf{S}_o^1, \mathbf{S}_o^2, \ldots, \mathbf{S}_o^{N_i}]^{\mathrm{T}}. \tag{14}$$

The entries of the submatrices are given by

$$\begin{aligned}[\mathbf{R}_o^{i_1,i_2}]_{rs} &= \sum_{f=1}^{N_f} |\mathrm{W}_o(\omega_f)|^2 F_{i_1}^*(\omega_f)F_{i_2}(\omega_f)\Omega_f^{r-1^{\mathrm{H}}}\Omega_f^{s-1},\\ [\mathbf{S}_o^{i_1}]_{rs} &= -\sum_{f=1}^{N_f} |\mathrm{W}_o(\omega_f)|^2 F_{i_1}^*(\omega_f)X_o(\omega_f)\Omega_f^{r-1^{\mathrm{H}}}\Omega_f^{s-1},\\ [\mathbf{T}_o]_{rs} &= \sum_{f=1}^{N_f} |\mathrm{W}_o(\omega_f)X_o(\omega_f)|^2 \Omega_f^{r-1^{\mathrm{H}}}\Omega_f^{s-1}.\end{aligned} \tag{15}$$

From Eqs. (13) and (15) it clearly follows that the submatrices of the normal matrix have a predefined structure. By exploiting the specific matrix structure, an important reduction of the computation time and memory requirements is obtained. More specifically, when a discrete-time model is used (i.e., $\Omega_f = \mathrm{e}^{(-\mathrm{i}\omega_f T_s)}$) the submatrices $\mathbf{R}_o$, $\mathbf{S}_o$ and $\mathbf{T}_o$ have a Toeplitz structure while

the entries can be computed by means of the fast Fourier transform (FFT) algorithm if the frequencies are uniformly distributed [14]. Using a discrete time-domain model leads to both a well-conditioned Jacobian and normal matrix. In the case of a continuous time-domain model, orthogonal polynomials have to be used to significantly improve the numerical conditioning [15,16].

Although the number of rows of the normal matrix in Eq. (13) is much smaller than the number of rows of the Jacobian matrix in Eq. (10), its size (i.e., $(n+1)(N_oN_i+1)$) is still often of importance for the computation time in the case of typical modal test data ($N_o > 100$) since solving Eqs. (13) for θ requires $(N_oN_in)^3$ flops.

Under the condition that the LS parameter constraint only applies to the denominator coefficients θ_A (e.g., by fixing highest order coefficient $a_n = 1$), the numerator coefficients θ_{B_o} can be eliminated from the normal equations by substitution of

$$\theta_{B_o} = -\mathbf{R}_o^{-1}\mathbf{S}_o\theta_A, \quad o = 1, \ldots, N_o, \tag{16}$$

in the last $(n+1)$ equations of Eq. (13), which yields a very compact problem

$$\left[\sum_{o=1}^{N_o} \mathbf{T}_o - \mathbf{S}_o^{\mathrm{H}}\mathbf{R}_o^{-1}\,\mathbf{S}_o\right]\theta_A = \mathbf{D}\theta_A \approx 0. \tag{17}$$

The square matrix $\mathbf{D}$ has a size $(n+1)$ and thus is much smaller than the original normal matrix in Eqs. (13) with size $(n+1)(N_oN_i+1)$. Once the denominator coefficients θ_A are known, a back-substitution can be used to find θ_B based on Eq. (16).

Similar to the well-known (polyreference) LSCE estimator, the results of this frequency-domain LS approach can be used to construct a stabilization chart in order to separate the physical poles (corresponding to a mode of the studied system) from the mathematical ones. To construct a stabilization chart, the poles have to be estimated for increasing model orders. To do this in an efficient way, the LSCE estimator first constructs a so-called "covariance matrix" for a given maximum model order [6]. Once formed, the LS problem can be solved for all smaller model orders by using sub-matrices of the full covariance matrix. The same idea can be applied to Eq. (17) where

$$\left[\sum_{o=1}^{N_o} \mathbf{T}_o - \mathbf{S}_o^{\mathrm{H}}\mathbf{R}_o^{-1}\mathbf{S}_o\right] \tag{18}$$

plays a similar role as the covariance matrix. By doing so, a set of LS solutions is obtained for a varying order of the denominator polynomial while the order of the numerator polynomials is kept constant and equal to the maximum specified order.

It turned out that the choice of LS constraint applied on the denominator coefficients to remove parameter redundancy in model (1), plays an important role in obtaining a clear stabilization chart. The best results were obtained by constraining the highest order coefficient of the denominator to one, i.e., a_n (see Section 4).

3.2. Maximum likelihood solver

The ML estimates of the polynomial coefficients are obtained by minimizing Eq. (5) with respect to these parameters θ. This can be done by means of a Gauss–Newton (or Levenberg–Marquard for improved convergence) optimization algorithm, which takes advantage of the quadratic form of the cost function (5). The Gauss–Newton iterations are given by

(1) solve the normal equations

$$\mathbf{J}_m^{\mathrm{H}}\mathbf{J}_m\delta_m = -\mathbf{J}_m^{\mathrm{H}}\mathbf{e}_m \quad \text{for } \delta_m \tag{19}$$

with $\mathbf{e}_m = \mathbf{e}(\theta_m)$, $\mathbf{J}_m = \partial\mathbf{e}(\theta)/\partial\theta|_{\theta_m}$ and $\mathbf{e}(\theta) = [\varepsilon_1^s, \ldots, \varepsilon_{N_o}^s]^{\mathrm{T}}$.

(2) compute an update of the previous solution θ_m

$$\theta_{m+1} = \theta_m + \delta_m. \tag{20}$$

However, when complex-valued coefficients are used, the equation error $\varepsilon_o^s(\Omega_f, \theta)$ in Eq. (5) is not analytical in the (complex) parameters θ and hence, the entries of the Jacobian matrix $\mathbf{J}_m$ can only be computed by considering the real and imaginary part of the coefficients as

$$\delta_m = [\mathrm{Re}(\delta_{B_1})^{\mathrm{T}}, \mathrm{Im}(\delta_{B_1})^{\mathrm{T}}, \ldots, \mathrm{Re}(\delta_A)^{\mathrm{T}}, \mathrm{Im}(\delta_A)^{\mathrm{T}}]^{\mathrm{T}}, \tag{21}$$

$$\mathbf{J}_{\mathrm{Re}_m} = \partial\mathbf{e}(\theta_{\mathrm{Re,Im}})/\partial\theta_{\mathrm{Re}}|_{\theta_{\mathrm{Re}_m,\mathrm{Im}_m}}, \quad \mathbf{J}_{\mathrm{Im}_m} = \partial\mathbf{e}(\theta_{\mathrm{Re,Im}})/\partial\theta_{\mathrm{Im}}|_{\theta_{\mathrm{Re}_m,\mathrm{Im}_m}}. \tag{22}$$

The entries in Eqs. (22) of the Jacobian matrix $\mathbf{J}_m$, for the weighted equation error at spectral line f, are found to be given as

$$\lfloor \mathbf{J}_{\mathrm{Re}_m,\mathrm{Im}_m} \rfloor_o = \frac{1}{\mathrm{var}(\varepsilon_o)^{1/2}} \frac{\partial\varepsilon_o}{\partial\theta_{\mathrm{Re,Im}}}\bigg|_{\theta_{\mathrm{Re}_m,\mathrm{Im}_m}} - \frac{1}{2}\frac{\varepsilon_o}{\mathrm{var}(\varepsilon_o)^{3/2}} \frac{\partial\,\mathrm{var}(\varepsilon_o)}{\partial\theta_{\mathrm{Re,Im}}}\bigg|_{\theta_{\mathrm{Re}_m,\mathrm{Im}_m}}, \tag{23}$$

where $\varepsilon_o(\Omega, \theta_{\mathrm{Re}_m,\mathrm{Im}_m})$ is denoted as ε_o.

Since the correlations between the outputs are omitted and a common denominator model (1) is used, the Jacobian matrix $\mathbf{J}_m$ in Eq. (21) has a similar block structure as the Jacobian matrix of the least-squares formulation in Eq. (10). As a result, the normal equations (i.e., $\mathbf{J}_m^{\mathrm{H}}\mathbf{J}_m$ and $\mathbf{J}_m^{\mathrm{H}}\mathbf{e}_m$ in Eq. (21)) are also structured matrices

$$\begin{bmatrix} \mathbf{R}_1 & 0 & \cdots & \mathbf{S}_1 \\ 0 & \mathbf{R}_2 & 0 & \mathbf{S}_2 \\ \vdots & 0 & \ddots & \vdots \\ \mathbf{S}_1^{\mathrm{H}} & \mathbf{S}_2^{\mathrm{H}} & \cdots & \sum_{o=1}^{N_o} \mathbf{T}_o \end{bmatrix} \begin{Bmatrix} \delta\theta_{B_1} \\ \delta\theta_{B_2} \\ \vdots \\ \delta\theta_{B_{N_o}} \\ \delta\theta_A \end{Bmatrix} = - \begin{bmatrix} \mathbf{\Gamma}_1^{\mathrm{H}}\varepsilon_1 \\ \mathbf{\Gamma}_2^{\mathrm{H}}\varepsilon_2 \\ \vdots \\ \mathbf{\Gamma}_{N_o}^{\mathrm{H}}\varepsilon_{N_o} \\ \sum_{o=1}^{N_o} \mathbf{\Phi}_o^{\mathrm{H}}\varepsilon_o \end{bmatrix}, \tag{24}$$

and hence it is again possible to construct these in a time-efficient way making use of the Toeplitz structure and FFT algorithm in the case that a discrete-time model is used. Furthermore, given the block structure of $\mathbf{J}_m$, the first N_o blocks can be eliminated from the normal equations analogously to the LS algorithm presented in Section 3.1.

A practical implementation of the ML algorithm for modal parameter estimation from IO data obtained by means of a SLDV, is often done when only the variances of the responses are taken

into account (i.e., $\mathbf{C}_F = 0$ and $\mathbf{C}_{FX_o} = 0$ in Eq. (6)). This can be justified by the fact that most important measurement errors are typically present on the outputs since occasional drops in laser beam reflection or spikes can result in important errors on some of the response signals.

While the cost function (5) is uniquely defined, this is not the case for the equation error $\varepsilon_o^s(\Omega_f, \theta)$ and hence the equation error $\varepsilon_o(\Omega_f, \theta)$ can be formulated as

$$\varepsilon_o(\Omega_f, \theta) = \lfloor \hat{\mathbf{H}}_o(\Omega_f, \theta) \rfloor \{\mathbf{F}(\omega_f)\} - X_o(\omega_f), \tag{25}$$

with $\lfloor \hat{\mathbf{H}}_o(\Omega_f, \theta) \rfloor = \lfloor \mathbf{B}_o(\Omega_f, \theta) \rfloor / A(\Omega_f, \theta)$ and the following expression for the variance

$$\mathrm{var}(\varepsilon_o(\Omega_f, \theta)) = \mathrm{var}(X_o(\omega_f)). \tag{26}$$

Weighting the equation error (25) by $\mathrm{var}(\varepsilon_o(\Omega_f, \theta))^{-1/2}$ results in an expression that is analytical in the complex polynomial coefficients θ. For this particular case, the Jacobian matrix J_m has the same structure as the Jacobian matrix in Eq. (10), with the submatrices $\mathbf{\Gamma}_{oi}$ and $\mathbf{\Phi}_o$ given by

$$\mathbf{\Gamma}_{oi} = \begin{bmatrix} \dfrac{\Omega^0(\omega_1)F_i(\omega_1)}{\sqrt{\mathrm{var}(X_o(\omega_1))}A(\omega_1, \theta)} & \cdots & \dfrac{\Omega^n(\omega_1)F_i(\omega_1)}{\sqrt{\mathrm{var}(X_o(\omega_1))}A(\omega_1, \theta)} \\ \vdots & \cdots & \vdots \\ \dfrac{\Omega^0(\omega_{N_f})F_i(\omega_{N_f})}{\sqrt{\mathrm{var}(X_o(\omega_{N_f}))}A(\omega_{N_f}, \theta)} & \cdots & \dfrac{\Omega^n(\omega_{N_f})F_i(\omega_{N_f})}{\sqrt{\mathrm{var}(X_o(\omega_{N_f}))}A(\omega_{N_f}, \theta)} \end{bmatrix}, \tag{27}$$

and

$$\mathbf{\Phi}_o = \begin{bmatrix} -\dfrac{\Omega^0(\omega_1)\lfloor \mathbf{B}_o(\omega_1, \theta) \rfloor \{\mathbf{F}(\omega_1)\}}{\sqrt{\mathrm{var}(X_o(\omega_1))}\,|A(\omega_1, \theta)|^2} & \cdots & -\dfrac{\Omega^n(\omega_1)\lfloor \mathbf{B}_o(\omega_1, \theta) \rfloor \{\mathbf{F}(\omega_1)\}}{\sqrt{\mathrm{var}(X_o(\omega_1))}\,|A(\omega_1, \theta)|^2} \\ \vdots & \cdots & \vdots \\ -\dfrac{\Omega^0(\omega_{N_f})\lfloor \mathbf{B}_o(\omega_{N_f}, \theta) \rfloor \{\mathbf{F}(\omega_{N_f})\}}{\sqrt{\mathrm{var}(X_o(\omega_{N_f}))}\,|A(\omega_{N_f}, \theta)|^2} & \cdots & -\dfrac{\Omega^n(\omega_{N_f})\lfloor \mathbf{B}_o(\omega_{N_f}, \theta) \rfloor \{\mathbf{F}(\omega_{N_f})\}}{\sqrt{\mathrm{var}(X_o(\omega_{N_f}))}\,|A(\omega_{N_f}, \theta)|^2} \end{bmatrix}. \tag{28}$$

Given the uncertainty on the measurements as defined in Eqs. (2), the covariance matrix of the ML estimate $\hat{\theta}_{ML}$ can be computed according the approximation

$$\mathbf{C}(\hat{\theta}_{ML}) \approx [\mathbf{J}_m^{\mathrm{H}}\mathbf{J}_m]^{-1}, \tag{29}$$

with $\mathbf{J}_m$ the Jacobian matrix evaluated in the last iteration step of the Gauss–Newton algorithm [17]. As the main interest is in the uncertainty on the modal frequencies and damping ratios, only the covariance matrix of the denominator coefficients is required. Starting from the previous approximation, it can be shown that this matrix is given by

$$\mathbf{C}(\hat{\theta}_A) \approx \left[\left(\sum_{o=1}^{N_o} \mathbf{T}_o - \mathbf{S}_o^{\mathrm{H}}\mathbf{R}_o^{-1}\mathbf{S}_o \right) \right]^{-1}, \tag{30}$$

with $\mathbf{R}_o$, $\mathbf{S}_o$ and $\mathbf{T}_o$ the submatrices of the normal equations $\mathbf{J}_m^{\mathrm{H}}\mathbf{J}_m$, similar as defined in matrix (13). Hence it is not necessary to invert the full covariance matrix of the normal equations $\mathbf{J}_m^{\mathrm{H}}\mathbf{J}_m$. Moreover, the covariance matrix (30) is the inverse of the matrix that is also computed to solve the normal equations that are obtained after elimination of the numerator coefficients from Eq. (19). Based on matrix (30), the uncertainty on the poles (modal frequencies and damping ratios) can be

derived [18]. Hence, confidence bounds are obtained together with the modal parameters, without the need for a Monte Carlo approach.

4. Experimental validation

4.1. Effects of excitation, data and noise model type on model accuracy

In a first case study, shaker excitation is used to measure an aluminium plate in 39 points by means of a SLDV set-up, as shown in Fig. 2. A random noise or multisine were used for shaker excitation in a band between 0 and 4096 Hz. Each period contains 8192 time samples. A second and unknown (unmeasured) excitation was generated by means of a loudspeaker producing random noise. A reference measurement was performed to obtain a so-called "true FRF" from

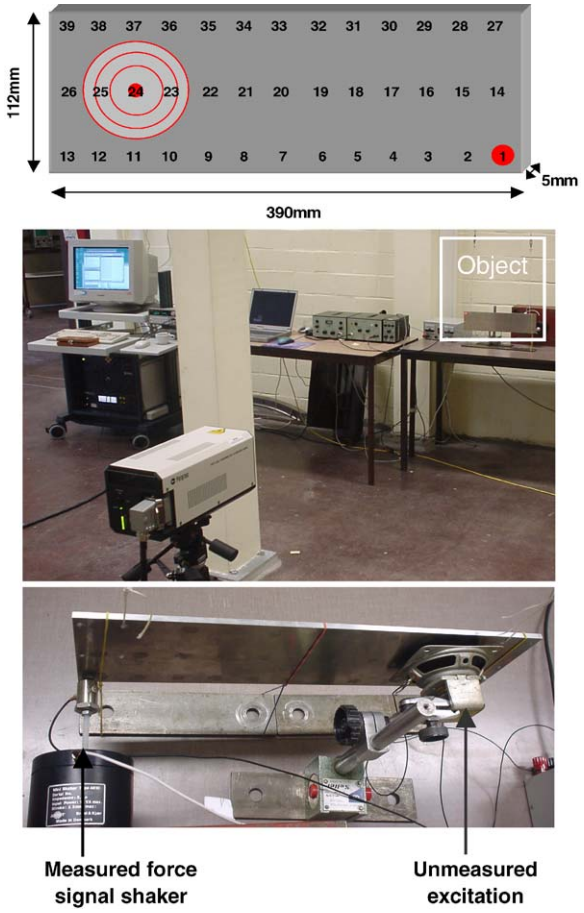

Fig. 2. Dimensions and excitation/response locations for Al-plate under test (top). Experimental SLDV setup (middle). Force (input) measurement with shaker, stinger and impedance head attached to the aluminum plate in point 1 and unmeasured acoustical excitation using loudspeaker around point 24 (bottom).

experimental data by averaging 10 periods acquired under a multisine excitation, while the loudspeaker was turned off. In this case the signal-to-noise ratios for the force and response spectra were around 40–50 dB. The errors-in-variables non-parametric FRF estimator, presented in H_{ev} [8], yielded a reference data set for evaluating the effects of the choice of excitation signal, type of data (IO vs. FRF) and use of noise covariance information on the model accuracy.

The effect of incorporating noise covariance information from an EV noise model is illustrated in Fig. 3 showing the amplitude and phase of a true FRF and the estimated model using IO data for multisine excitation with a high level of process noise generation by the loudspeaker, resulting in poor signal-to-noise ratios the force and response spectra around 5–10 dB. In fact, the actual FRFs are very noisy, which complicates the model estimation and leads to very poor results in the case of the traditional curve fitting schemes. By taking into account knowledge about the uncertainty on the data, the IO ML estimator still succeeds in estimating an accurate transfer function model very well. The benefits of using additional information about the data can be clearly observed from the comparison of the transfer function models when considering the EV model or not. The variances of the input and output Fourier series are easily obtained by means of a sample variance computation since the signals are acquired using periodic (multisine) excitation.

In general, all modes are significantly better estimated by means of the proposed IO ML estimator and this is especially so for the modes at 463 and 1256 Hz. Obviously, this also has its

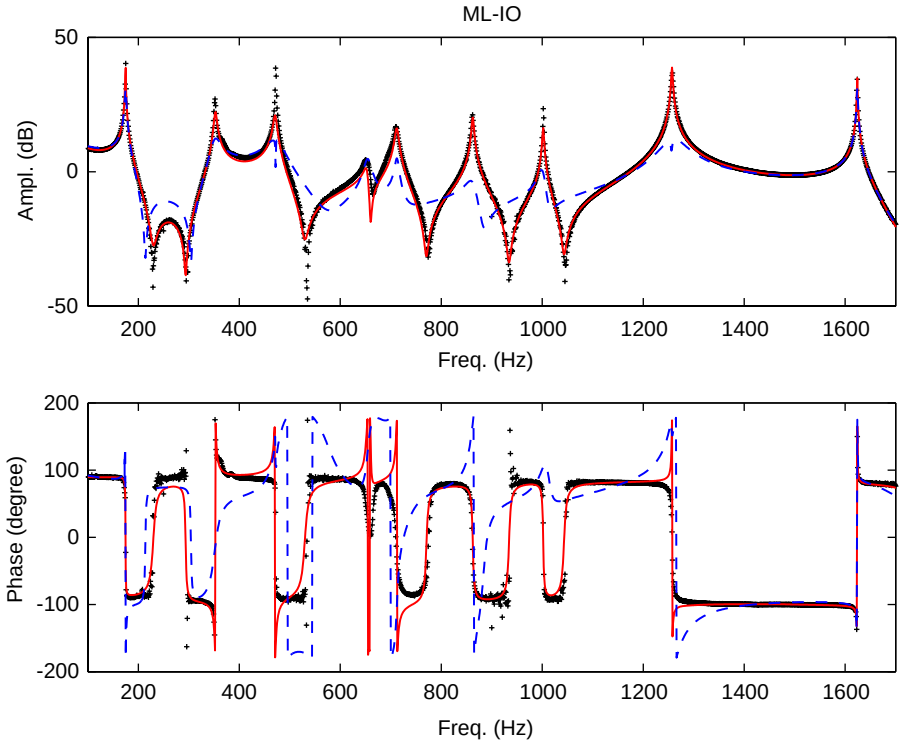

Fig. 3. Amplitude and phase of true FRF (+) and synthesized model obtained from Fourier IO data under multisine excitation for high level of extraneous noise source (loudspeaker). Improved accuracy by incorporation of EV noise model (solid) compared to not using noise covariance information (dashed).

implications for the mode shapes. For example the mode around 1256 Hz can only be clearly identified if the appropriate noise model is taken into account, as illustrated in Fig. 4.

The error on each of the estimated modes significantly increases for a poor mode excitation and a significant feedback of the extraneous (unmeasured) noise source in the measured force signal. Both effects result in noise on the data, which can only be treated well by taking this data uncertainty into account during the ML estimation.

The influence of the excitation signal used is illustrated in Fig. 5, showing the amplitude and phase of true FRF and the estimated model using the H_1 FRF data obtained for a multisine and random noise excitation, for a high level of random noise produced by the loudspeaker. The FRF data is processed using the FRF ML estimator [11], where the variance for each of the H_1 FRF is computed from its coherence function. The choice of a broadband periodic excitation, such as a multisine signal, has important benefits with respect to the final model accuracy. Better signal-to-noise ratios and leakage-free signal processing yield better data quality compared with random noise excitation and for the same number of acquired data samples.

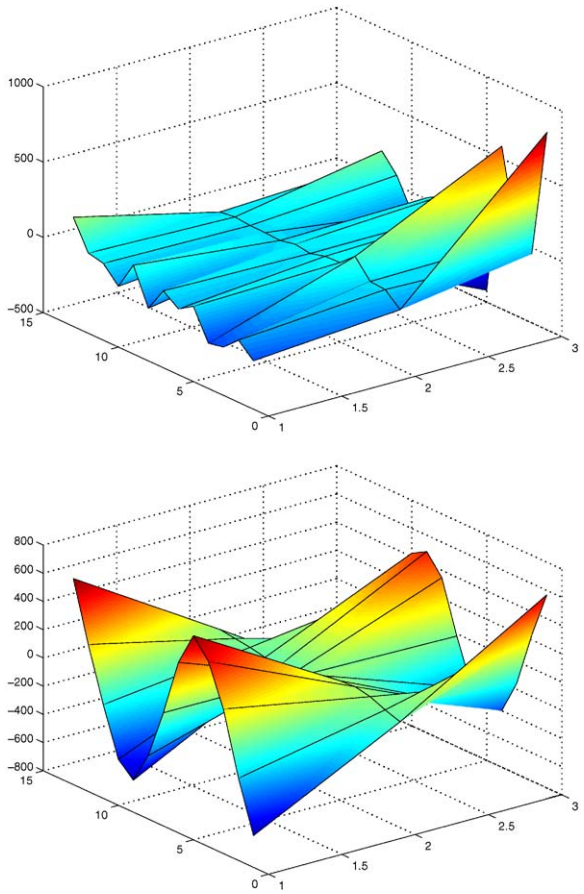

Fig. 4. Comparison of mode at 1256 Hz in model obtained from IO data under multisine excitation without (top) and with (bottom) including EV noise model.

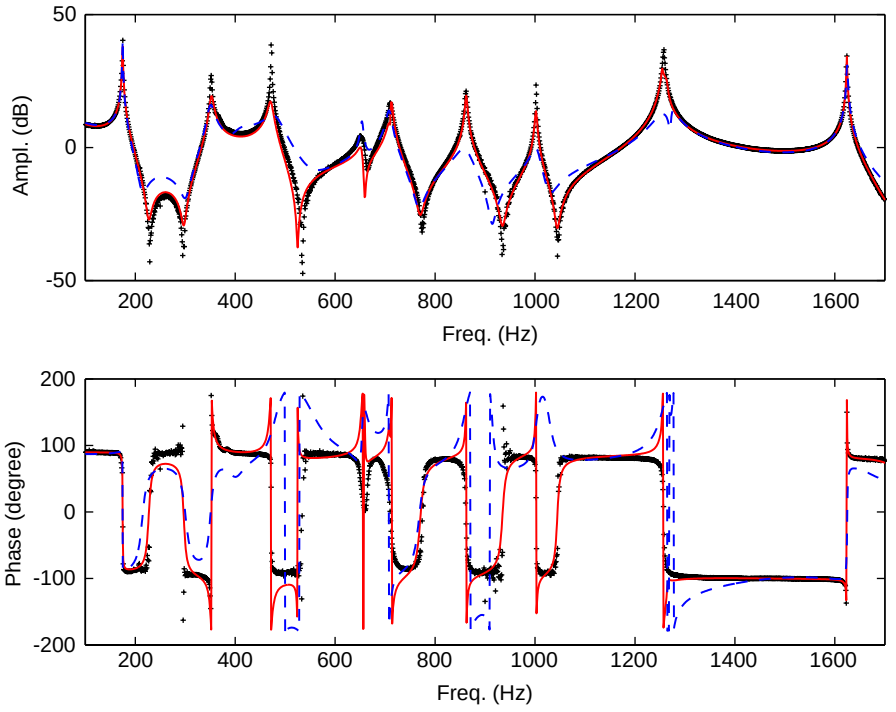

Fig. 5. Amplitude and phase of true FRF (+) and synthesized model obtained from H_1 FRF data under multisine (solid) and random noise (dashed) excitation for high level of extraneous noise source (loudspeaker).

Using multisine excitation, the use of IO data further improves the accuracy since a much more accurate noise model is taken into account compared to FRF data, which is computed under H_1 noise assumptions introducing to some extent bias errors in experimental FRF data. This is illustrated in Fig. 6 giving the amplitude and phase of true FRF and the estimated models obtained for multisine excitation using (H_1) FRF and IO data. The most important differences appear at the frequencies corresponding with the resonances of the system, which however are most important for modal analysis. Amplitude differences up to 10 dB can still be seen, explained by errors in the FRF data.

Remark. In order to preserve the clarity of the presentation of the results, only the first part of the frequency band 0–4 kHz has been shown in Figs. 3, 5 and 6. However, it is should be noted that the IO ML estimator, presented in Section 3.2, is very robust for high model orders (up to 100 modes, by the use of discrete-time model) and hence it was possible to accurately analyse the total frequency band (containing around 40 modes) in a single MLE analysis.

4.2. Stabilization diagram, computation speed and leakage modelling

A second case study deals with modal test data obtained from a slat track of an Airbus A320 commercial aircraft. Slat tracks are located at the leading edge of an aircraft wing and form part

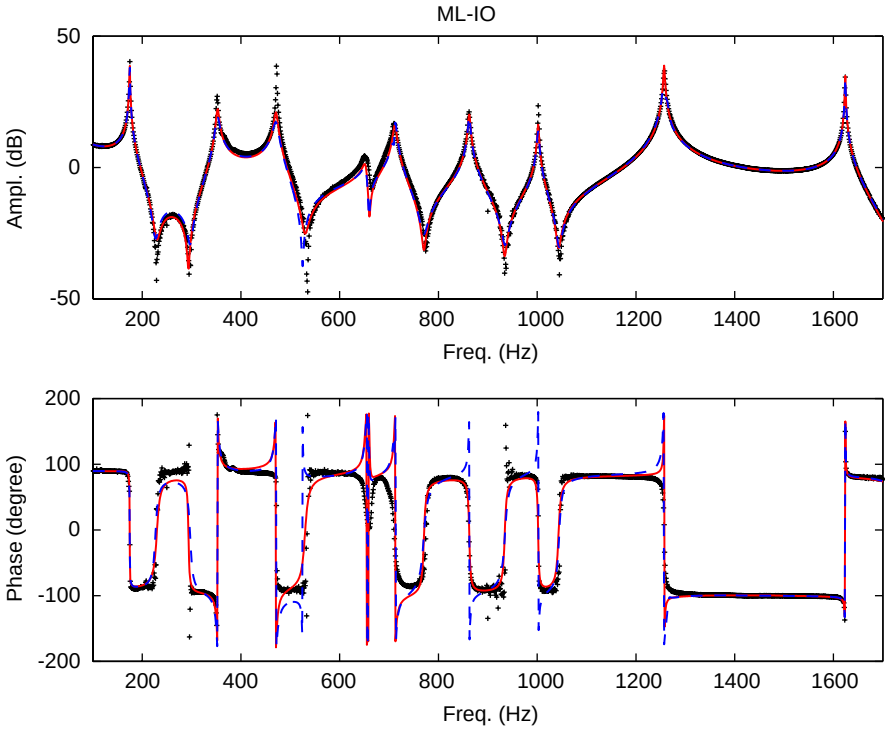

Fig. 6. Amplitude and phase of true FRF (+) and synthesized model obtained from Fourier IO (solid) and H_1 FRF (dashed) data under multisine excitation for high level of extraneous noise source (loudspeaker).

Fig. 7. A Slat track mounted in the wing of an Airbus320 aircraft.

of a gliding mechanism that is used to enlarge the wing surface (see Fig. 7). The enlargement of the wing surface is needed to increase the lift force at reduced velocity during landing and take off.

Fig. 8 shows the experimental setup. An electrodynamic shaker was used to apply a multisine or a random noise excitation in the frequency band 0–4000 Hz with 16,384 frequency lines. The time histories of the applied force and response (acceleration) were measured using an impedance head.

A model with 22 modes was estimated in the frequency band 250–1500 Hz containing 1000 spectral lines. Fig. 9 shows the velocity/force ratio of the Fourier transformed signals (dots) and

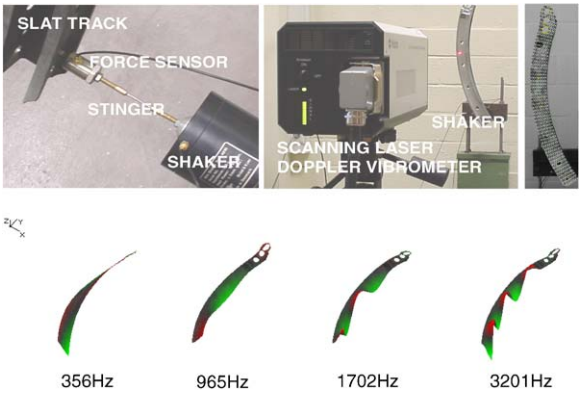

Fig. 8. Force (input) measurement with shaker, stinger and impedance head attached to the slat track (top, left). Velocity measurement with SLDV in grid of 352 points (top, middle & right). Some mode shapes of the slat track with bending and torsional behavior (bottom).

the model (solid) estimated by the IO least-squares (top) and IO maximum likelihood (bottom) solvers. The ML approach is more suited to deal with SLDV measurements that are partially corrupted by spikes and poor reflection (when beam targets on edge of ribs on component) that introduce measurement errors.

However, as a starting values estimator, the fast IO least-squares estimator (see Section 3.1) also enables the fast construction of stabilization charts. Fig. 10 shows the stabilization diagram for the LSCE (top) and the weighted IO LS frequency-domain estimator (bottom) with (+) stable and (•) unstable poles (i.e., with positive real part). Both the use of a proper weighting function, i.e., $\mathbf{W}_o(\omega_f) = \mathrm{var}(X_o(\omega_f))^{-1}$ in Eq. (10), and the fixation of the highest order denominator polynomial coefficient ($a_n = 1$), generally result in clear stabilization charts for the IO weighted LS (WLS) yet with an acceptable accuracy for data sets with reasonable noise levels.

Fig. 11 compares the full ML (without use of elimination) and fast ML (denoted as FML, presented in Section 3.2) algorithms in terms of flops count, for a varying number of outputs N_o (with $N_m = 20$, $N_i = 1$) and a varying model order N_m (with $N_o = 10$, $N_i = 1$). Considering the output dimension N_o, the results indicate that one iteration of the full ML problem is solved in $\mathcal{O}(N_o^3)$ flops, whereas $\mathcal{O}(N_o)$ flops for one iteration of the FML, resulting in a gain of $\mathcal{O}(N_o^2)$ flops, explained by the elimination approach. On the other hand, for an increasing model order, the number of flops used by the ML and FML is similar, i.e., $\mathcal{O}(N_m^3)$.

The use of a transient polynomial is illustrated using this slat track data. Using the IO data obtained by the multisine, an ML estimate of the transfer function model is used as reference data. As a first case, the complete random noise time records (number of time samples $N_s = 32,768 = 32$ K) were considered. Fig. 12(a) compares the model obtained by the IO ML estimator using the FFT of the time records, when using a transient polynomial or not. The dashed–dotted line corresponds to the reference model obtained from the multisine data. The (non-parametric) empirical transfer function estimate (ETFE [19]) (dots), computed as the ratio of the output and input Fourier spectra, is a very noisy function as can be expected. From these data, the IO ML estimator yielded a model without (dashed line) and with using a transient polynomial

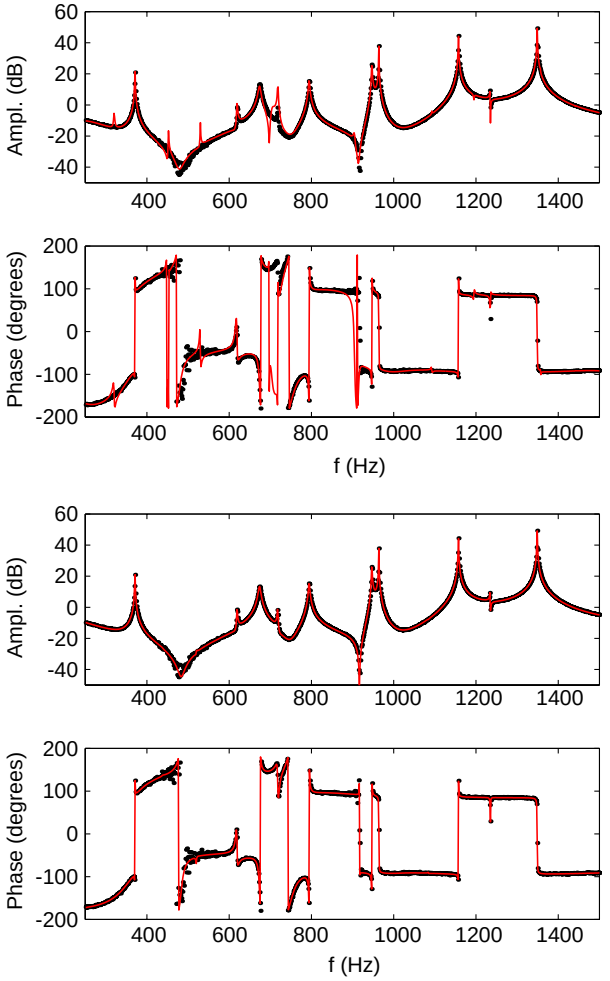

Fig. 9. Amplitude and phase of IO data (•) and estimated transfer function model for slat track using IO LS (top) and IO ML (bottom) estimators.

(solid line). A model with 30 modes was estimated for a frequency band 200–1500 Hz. By zooming in, the effects of leakage can already be noticed when no transient polynomial is used, as for instance for the mode at 1156 Hz. In this case the zoomed frequency band has 921 spectral lines ($N_f = 921$). Decreasing the size of the records clearly introduces more leakage effects in the case of random noise data, as is shown in Fig. 12 for $N_s = 8$ K ($N_f = 231$ in zoom) (b) and $N_s = 2$ K ($N_f = 59$) (c). As can be seen for this experimental case, the approach using the IO ML with transient polynomial is very robust for short data records. Even in the case of 2 time samples corresponding to a frequency resolution of 4 Hz, this approach can still estimate an accurate model compared to the approach without using this transient polynomial.

The IO ML approach can also be compared with the FRF-based ML [11]. The FRF data can be obtained either by computing a H_1 estimate, which however requires the averaging of a number of subrecords, or by computing the ETFE also using a Hanning window. Since, in the general case

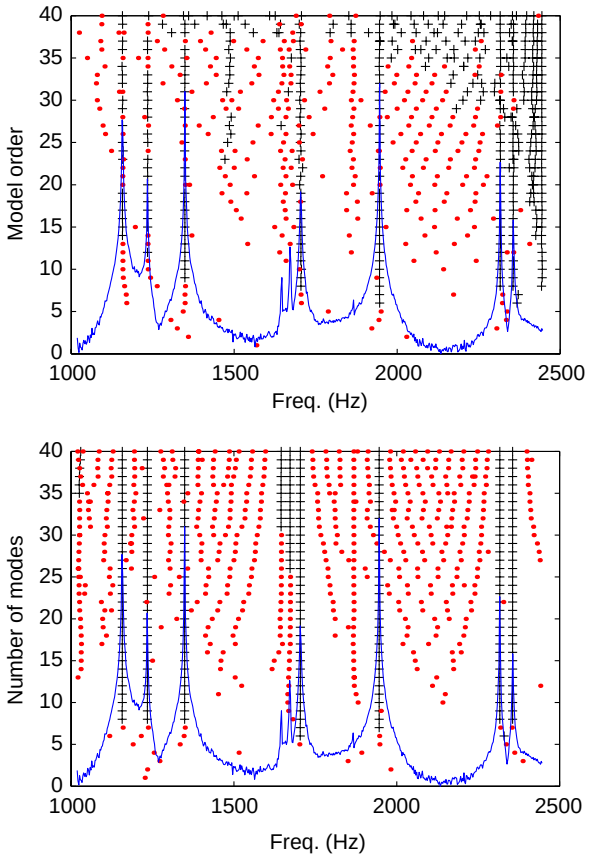

Fig. 10. Stabilization diagram for LSCE (top) and IO WLS (highest order $a_n = 1$) (bottom) with (+ = stable), (• = unstable, i.e., positive real part) and (solid = averaged sum FRFs).

of short data records, the first possibility is not applicable, a comparison was done using the ETFE. Fig. 13 shows a zoom on the results found when using the FRF ML for the same analysis parameters as for the IO estimation for a decreasing size of the records. As can be seen, the estimated model is acceptable in the case of the 32 K samples; however, due to important leakage errors the results quickly deteriorate for a decreasing blocksize when compared to the IO ML approach that also models the transient effects. The use of a Hanning window is not sufficient once the records become short, in this case $N_s = 2$ K or less.

4.3. *Improvements for flight flutter data analysis*

In this section the case of flight flutter testing will be considered to validate the IO ML algorithm for very noisy data. The classical flight flutter testing approach consists of expanding the flight envelope of an airplane by performing a vibration test at constant flight conditions, curve-fitting the data to estimate the resonance frequencies and damping ratios, and then

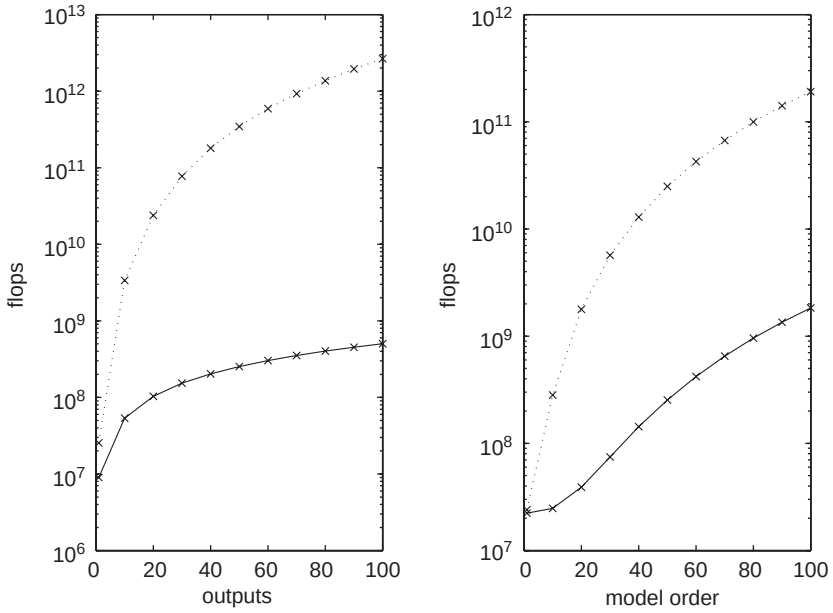

Fig. 11. Flops count for full ML (dashed) and fast ML (solid) implementation for varying number of outputs and $N_m = 20$ (left) and varying model order and $N_o = 10$ (right).

monitoring these frequencies and damping estimates against flight speed or Mach number. The damping values are then extrapolated in order to determine whether it is safe to proceed to the next flight test point. However, it is well known that it is usually quite difficult to obtain accurate estimates of damping ratios. Consequently, having confidence intervals on the damping estimates should make the decision to proceed to the next test condition more reliable.

To illustrate the possibilities of the ML estimator for very noisy data, it is now applied to flight flutter data. Here noise means the effects of unmeasured forces, such as turbulence effects, that act on the airplane. Since these effects are found only in the responses, this results in very noisy data. Nevertheless, by taking knowledge about this noise into account by means of the ML estimator according to an EV model it is still possible to obtain accurate modal parameters.

Based on a SISO measurement consisting of 3 swept-sine bursts, the Fourier IO data and corresponding noise covariance matrix is obtained as the sample mean and variance over the 3 bursts. Fig. 14 shows the IO data presented as the ETFE and the synthesized transfer function model estimated by the IO WLS and IO ML solvers. Comparing these results, it is concluded that the quality of the model estimated by the maximum likelihood estimator is superior to the least-squares approach for flight flutter modelling, especially for the mode at 6.2 Hz which is very difficult to estimate due to high noise levels. Actually, this mode is less well excited by the excitation device (rotating vane) resulting in a poor contribution of this mode in the response dominated by the noise on the data. Using a proper weighting function for the LS estimator, i.e.,

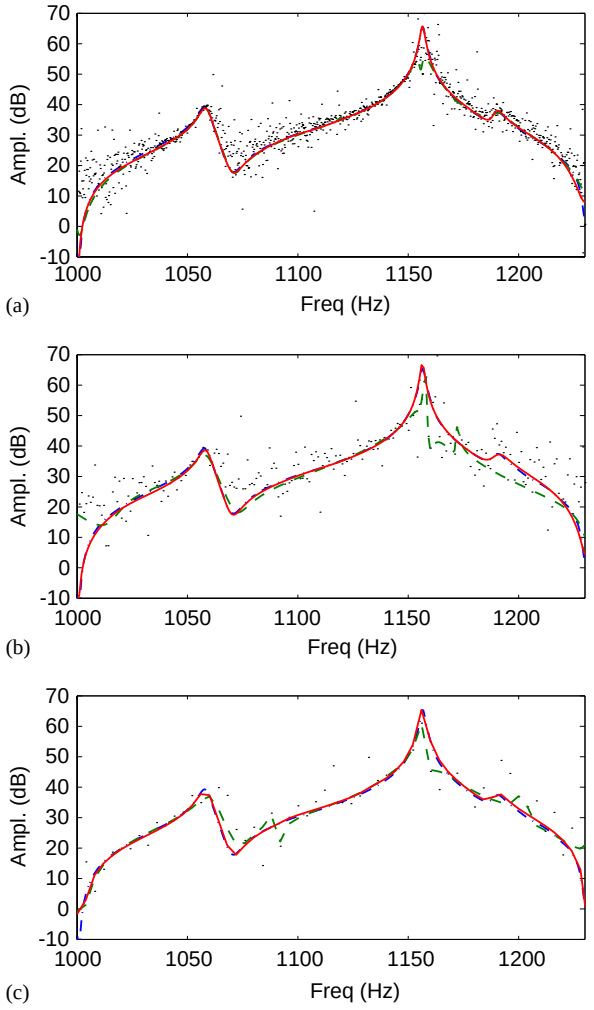

Fig. 12. Comparison of IO ML results without (dashed) and with (solid) transient polynomial with reference model (dashed–dotted) and the ETFE for random noise Fourier data (dots) - cases: $N_s = 32$ K ($N_f = 921$ in zoom) (a), $N_s = 8$ K ($N_f = 231$) (b) and $N_s = 2$ K ($N_f = 59$) (c).

$W_o(\omega_f) = \text{var}(X_o(\omega_f))^{-1}$ in Eq. (10), clearly improves the quality of the starting values and hence reduces the number of required ML iterations needed for a proper convergence.

5. Conclusions

In this paper the applicability of the frequency-domain maximum likelihood estimator has been improved for modal parameter estimation based on input–output Fourier data. Depending on the application, the use of advanced identification methods certainly improves the model accuracy by taking additional information about the errors on data into account. If required, the proposed

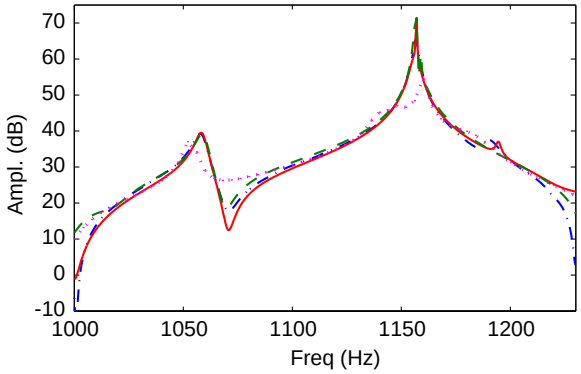

Fig. 13. Comparison of FRF (ETFE with Hanning window) ML results with reference model (dashed–dotted)—cases: $N_s = 32$ K ($N_f = 921$ in zoom) (solid), $N_s = 8$ K ($N_f = 231$) (dashed) and $N_s = 2$ K ($N_f = 59$) (dotted).

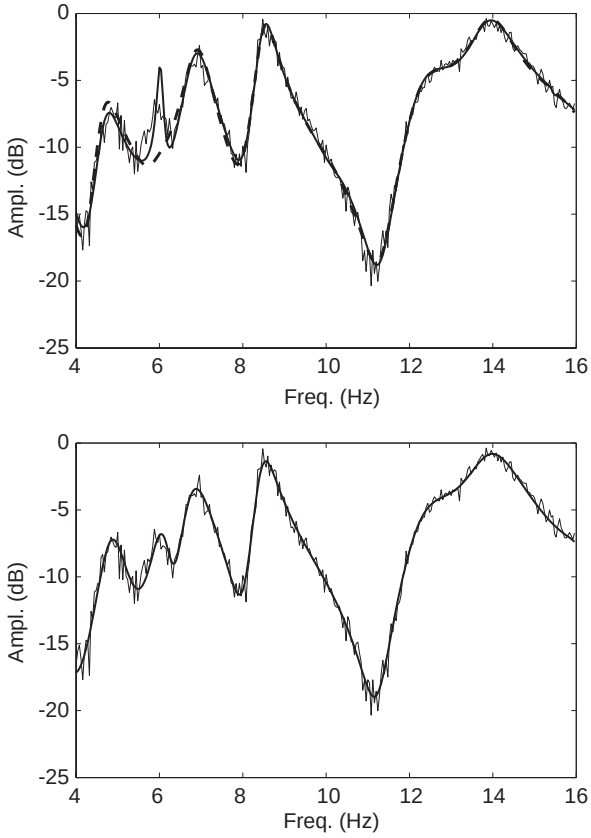

Fig. 14. IO data (ETFE) and synthesized FRF obtained by LS (top, dashed), WLS (top, solid) and ML (bottom) estimators.

maximum likelihood estimator also allows the simultaneous derivation of confidence bounds. Besides the advantages of better signal quality and leakage-free signal processing, the use of broadband excitation signals (e.g., multisine, periodic chirp) enables a fast determination of the noise covariance information for an errors-in-variables noise model.

The numerical optimization made the ML estimator suitable for handling large modal data sets with high modal density. Elimination and substitution procedures, algebraic and matrix properties and fast signal processing techniques are optimally applied in the implementation in order to handle large data sets in a reasonable time.

When random noise excitation is required, IO-based frequency-domain identification enables a parametric compensation for the effects of leakage by estimating the initial (and final) conditions together with the system parameters. This makes this estimator very robust for cases with short data records measured under arbitrary excitation.

Acknowledgements

This research is supported by grants from several funding agencies and sources: EUREKA FLITE project 2419; the Institute for the Promotion of Innovation by Science and Technology in Flanders (IWT); the Concerted Research Action "OPTIMech" of the Flemish Community; the Research Council (OZR) of the Vrije Universiteit Brussel (VUB).

Appendix A. Nomenclature

d.o.f.	degrees of freedom
ETFE	empirical transfer function estimate
EV	errors-in-variables
FFT	fast Fourier transform
FRF	frequency response function
FML	fast maximum likelihood
H_1	output-noise only FRF estimator
H_v	scaled FRF estimator
H_{iv}	instrumental variables FRF estimator
H_{ev}	errors-in-variables FRF estimator
IO	input/output
IV	instrumental variables
LS	least squares
LSCE	least-squares complex exponential
MIMO	multiple input multiple output
ML	maximum likelihood
MLE	maximum likelihood estimator
SDOF	single degree of freedom
SISO	single input single output
SLDV	scanning laser Doppler vibrometer
WLS	weighted least squares

References

[1] N.M.M. Maia, J.M.M. Silva (Eds.), *Theoretical and Experimental Modal Analysis*, Research Studies Press, Somerset, 1997.

[2] W. Heylen, S. Lammens, P. Sas, *Modal Analysis Theory and Testing*, PMA, KU Leuven, Leuven, Belgium, 1998.

[3] J.J. Juang, *Applied System Identification*, Prentice-Hall, Englewood Cliffs, NJ, 1994.

[4] M.H. Richardson, D.L. Formenti, Global curve fitting of frequency response measurements using the rational fraction polynomial method, in: *Proceedings of the Third International Modal Analysis Conference*, Orlando, FL, 1985, pp. 390–397.

[5] H. Van der Auweraer, J. Leuridan, Multiple input orthogonal polynomial parameter estimation, *Mechanical Systems and Signal Processing* 1 (3) (1987) 259–272.

[6] LMS International NV. *LMS CADA-X Manuals—Modal*, 2002.

[7] B.D.O. Anderson, Identification of scalar errors-in-variables models with dynamics, *Automatica* 21 (6) (1985) 709–716.

[8] P. Guillaume, Errors-in-variables identification techniques applied to modal analysis, in: *Proceedings of Design Engineering Technical Conferences (DETC)*, Sacramento, CA, ASME, New York, 1997, pp. DETC97/VIB-4253.

[9] P. Verboven, P. Guillaume, M. Van Overmeire, Improved modal parameter identification by non-parametric modeling of the measurement noise, in: *Proceedings of the 17th International Modal Analysis Conference*, Kissimmee, FL, 1999, pp. 1984–1990.

[10] P. Verboven, Frequency-domain System Identification for Modal Analysis, Ph.D. Thesis, vakgroep WERK, VUB, Brussel, Belgium, May, 2002.

[11] P. Guillaume, P. Verboven, S. Vanlanduit, Frequency-domain maximum likelihood identification of modal parameters with confidence intervals, in: *Proceedings of the 23rd International Seminar on Modal Analysis*, Leuven, Belgium, 1998, pp. 359–366.

[12] P. Guillaume, R. Pintelon, J. Schoukens, Description of a parametric MLE in the frequency domain for MIMO systems and its application to flight flutter analysis, *Mechanical Systems and Signal Processing* 4 (5) (1990) 405–416.

[13] R. Pintelon, J. Schoukens, G. Vandersteen, Frequency-domain system identification using arbitrary signals, *IEEE Transactions on Automatic Control* 42 (12) (1997) 1717–1720.

[14] P. Guillaume, R. Pintelon, J. Schoukens, I. Kollar, Crest-factor minimization using nonlinear Chebyshev approximation methods, *IEEE Transactions on Instrumentation and Measurements* 40 (6) (1991) 982–989.

[15] Y. Rolain, R. Pintelon, K.Q. Xu, H. Vold, Best conditioned parametric identification of transfer function models in the frequency domain, *IEEE Transactions an Automatic Control* 40 (11) (1995) 1954–1960.

[16] R. Pintelon, Y. Rolain, A. Bultheel, M. Van Barel, Numerically robust frequency domain identification of multivariable systems, in: *Proceedings of International Seminar on Modal Analysis (ISMA)*, Leuven, Belgium, 2002, pp. 1315–1321.

[17] R. Pintelon, J. Schoukens, *System Identification: A Frequency Domain Approach*, IEEE Press, New York, 2001.

[18] P. Guillaume, J. Schoukens, R. Pintelon, Sensitivity of roots to errors in the coefficient of polynomials obtained by frequency-domain estimation method, *IEEE Transactions on Instrumentation and Measurement* 38 (6) (1989) 1050–1056.

[19] L. Ljung, *System Identification: Theory for the User*, 2nd Edition, Prentice-Hall, Upper Saddle River, NJ, 1999.